

Cross-Shell Excitation in F and Ne Isotopes around $N = 20$

Menglan Liu  and Cenxi Yuan * 

Sino-French Institute of Nuclear Engineering and Technology, Sun Yat-sen University, Zhuhai 519082, China; liumlan3@mail2.sysu.edu.cn

* Correspondence: yuancx@mail.sysu.edu.cn

Abstract: Within the framework of the configuration–interaction shell model, the present work applies three effective interactions to investigate the effects of the cross-shell excitation on F and Ne isotopes around $N = 20$, which are significantly proton–neutron asymmetric, and have different properties compared with the proton–neutron symmetric nuclei. It is shown that cross-shell excitation is necessary in order to reproduce separation energies, neutron drip lines, and low-energy levels of these isotopes. Furthermore, the cross-shell excitation of $(0-5)\hbar\omega$ is suggested to be important in the description of ^{29}F and ^{30}Ne . However, the three interactions are insufficient in describing the bound structure of $^{29,31}\text{Ne}$, and provide inconsistent shell structures and evolutions in the target nuclei. Their cross-shell interactions are suggested to be improved.

Keywords: cross-shell excitation; F; Ne nuclei; $N = 20$ shell



Citation: Liu, M.; Yuan, C. Cross-Shell Excitation in F and Ne Isotopes around $N = 20$. *Symmetry* **2021**, *13*, 2167. <https://doi.org/10.3390/sym13112167>

Academic Editors: Yu-Gang Ma, De-Qing Fang and Fu-Rong Xu

Received: 29 September 2021
Accepted: 8 November 2021
Published: 12 November 2021

Publisher's Note: MDPI stays neutral with regard to jurisdictional claims in published maps and institutional affiliations.



Copyright: © 2021 by the authors. Licensee MDPI, Basel, Switzerland. This article is an open access article distributed under the terms and conditions of the Creative Commons Attribution (CC BY) license (<https://creativecommons.org/licenses/by/4.0/>).

1. Introduction

Nuclei with neutron numbers close to 20 are of interest. According to the conventional shell model, the $N = 20$ shell is closed, defining the boundary between the *sd* shell and the *pf* shell [1,2]. As a result, nuclei with $N = 20$ should be magic, which is valid for nuclei near the β -stability line, where protons and neutrons are almost symmetrical in the light nuclear region. However, for lighter elements, such as F [3], Ne [4–6], Na [7], and Mg [8], it is known that the $N = 20$ shell gap vanishes in extremely proton–neutron asymmetric nuclei, leading to the existence of the “island of inversion” [7]. Moreover, the neutron drip lines of C, N, and O have 16 neutrons [9–11], while ^{31}F and ^{34}Ne are the heaviest bound isotopes of F and Ne, respectively [12]. The abrupt change of the neutron drip line also manifests the evolution of the $N = 20$ shell. Since ^{29}F and ^{30}Ne are the two lightest bound nuclei with $N = 20$, a systematic study on the F and Ne isotopes around ^{29}F and ^{30}Ne is significant.

F and Ne isotopes with $N \sim 20$ are challenging to study due to their extreme proton–neutron asymmetry. For instance, ^{31}F has been known to be bound since 1999 [13], while the unbound character of $^{32,33}\text{F}$ was not determined until 2019 [3]. In fact, to date, only the masses of the F (Ne) isotopes with mass numbers less than 30 (32) have been experimentally determined [14]. On the other hand, some interesting phenomena in such nuclei have been experimentally discovered in recent years. For example, the “island of inversion” has been extended with several F and Ne isotopes [3,15], and exotic properties of F and Ne isotopes in the $N \sim 20$ region have been discovered [16,17]. In 2020, the two-neutron halo structure in ^{29}F [18] was experimentally identified. In 2021, neutron-unbound states were experimentally explored in ^{31}Ne [19]. Therefore, theoretical models can be helpful to investigate the extremely neutron-rich F and Ne nuclei.

There usually are three types of theoretical models of nuclear structure: the *ab initio* theories [20,21], mean-field approaches [22], and shell models [1,2,23]. All three have been employed for neutron-rich F and Ne nuclei [5,24–26]. In the past two years, various theoretical models considering the continuum coupling for nuclei near the drip line—including the coupled-cluster method [18], Gamow shell model [27], and Green’s function

method in the complex-momentum representation [25]—have been used to investigate the halo structure in $^{29,31}\text{F}$. Three-body systems have been built to analyze such exotic structures [28,29]. Nevertheless, a systematic study can be helpful to understand such unexpected phenomena.

The shell model is an essential tool for the systematic understanding of the nuclear structure. Recently, it has been employed in describing light, proton-rich, exotic nuclei and the related isospin symmetry breaking [30–33], interpreting the shell evolution in the medium mass region [34,35], reproducing isomeric states in the medium [36,37] and heavy nuclei [38–40], and investigating the α -decay properties of heavy-mass nuclei [41,42].

Within the shell model framework, it should be noticed that pure *sd*- or *pf*-shell model space is insufficient to study F and Ne isotopes around $N = 20$, due to the vanishing of the $N = 20$ shell gap. On this basis, the neutron excitation across the $N = 20$ shell is rather crucial. Fukunishi et al. employed an interaction in the model space, including the whole *sd* shell and the $0f_{7/2}$ and $1p_{3/2}$ orbits, and calculated some properties of ^{30}Ne , ensuring the necessity of cross-shell excitation [43]. The SDPF-M interaction, proposed by Utsuno et al., was presented with its results on the average neutron occupancy in the *pf* shell of even-mass $^{26-34}\text{Ne}$ [44]. Caurier et al. proposed the SDPF-U-MIX interaction, and showed the results of $^{29,31}\text{F}$ and $^{30-32}\text{Ne}$, considering the contribution of the particle-hole states in [45].

In fact, cross-shell excitation is not a fresh idea; just as near the $N = 20$ shell, it can also be seen in the $N = 8$ and $N = 28$ shells. For example, shell model calculations with the YSOX interaction have succeeded in reproducing the properties of neutron-rich Be [46,47], B [48], C [49,50], and O [51] isotopes with the help of the cross-shell excitation beyond $N = 8$. In the *sd* region, the interpretation of the exotic β - γ - α decay mode in ^{20}Na [52] also requires the neutron cross-shell excitation. Moreover, shell model studies with the SDPF-MU [53] and SDPF-U-SI [54] interactions were performed to describe the exotic Mg [55], Si [56], and S [53,54] isotopes, considering the neutron excitation across the $N = 28$ shell.

Despite the previous studies, a systematic investigation of the influences of cross-shell excitation on F and Ne isotopes around $N = 20$ is lacking. It would be interesting to know, for example, how many neutrons of cross-shell excitation should be considered if we wish to reproduce the neutron drip line of F and Ne. For this purpose, based on the widely used configuration–interaction shell model (CISM), this paper applied three different interactions—SDPF-M, SDPF-MU, and SDPF-U-SI—to investigate the role of the cross-shell excitation in the F and Ne isotopes with $N \sim 20$.

The paper is organized as follows: in the next section, CISM is briefly introduced, and the details of the three interactions are given; then, the results from the shell model calculations are shown to analyze the effects of the cross-shell excitation on the F and Ne neutron-rich isotopes; finally, a summary is presented.

2. Theories

The nuclear structure problem is essentially a many-body quantum problem, where protons and neutrons interact in a complex manner. To this end, CISM assumes an inert core, and defines a model space where the remaining nucleons can occupy the orbits. In the truncated model space, the effective Hamiltonian—also called the effective interaction—can be built from the nuclear force. Usually, the nuclear force can be derived from either the nucleon–nucleon scattering experimental data [57] or the observed nuclear structure data [58], called realistic nuclear force and phenomenological nuclear force, respectively. The former starts in a more *ab initio* manner, which needs to deal with hard-core and in-medium effects before the utilization. On the other hand, the phenomenological nuclear force depends a lot on experiments. The three effective interactions applied in this work are all constructed in a phenomenological manner. They can partially include continuum-coupling effects and proton–neutron asymmetry via fitting nuclear structure data of nuclei near the drip line. Then, through diagonalizing the Hamiltonian matrix, which consists of single-particle energies (SPEs) and two-body matrix elements (TBMEs), the wavefunc-

tions can be derived as eigenstates of the many-body Schrodinger equation. As a result, configuration-mixing is used to express each state.

There are normally three steps to perform CISM calculations in practice: The first step of CISM is to choose an appropriate model space. The second step, which is also the most critical step, is to construct the effective interaction in the model space. Finally, the shell model codes are used to diagonalize the Hamiltonian matrix. In this paper, the size of the model space is discussed by analyzing the effects of the cross-shell excitation. The input of the effective interaction is varied with three choices, while all of the calculations are performed with the code KSHELL [59–61].

To reproduce the structure of F and Ne isotopes around $N = 20$, the model space includes not only the sd -shell orbits, but also two or all pf -shell orbits. On this basis, the size of the model space can be further determined by restricting the number of neutrons of cross-shell excitation. Then, the interactions involving two major shells are divided into three parts: the sd -shell part, the pf -shell part, and the cross-shell part. The two former terms are based on well-known interactions in the sd - and pf -shell model space. Thus, the interactions constructed in the larger space can immediately describe the $N \sim Z$ nuclei. As for F and Ne nuclei around $N = 20$, the cross-shell interactions can be crucial, since both the sd - and pf -shell configurations contribute significantly to these nuclei. In the following subsections, the details of the three interactions will be described.

2.1. SDPF-M

The SDPF-M interaction was proposed by Utsuno et al. for studying neutron-rich nuclei with nearly 20 neutrons [44]. The interaction takes ^{16}O as the inert core, and considers the model space consisting of the full sd shell and the $0f_{7/2}$ and $1p_{3/2}$ orbits; it uses the USD interaction [62] and the KB interaction [63] for the sd -shell and pf -shell parts, respectively. More importantly, its cross-shell part starts from the MK interaction [64].

In detail, the MK interaction is close to a G-matrix interaction in character, except that MK has a repulsive triplet-odd central force. Warburton et al. [65] modified the eight TBMEs $\langle 0f_{7/2}0d_{3/2} | V | 0f_{7/2}0d_{3/2} \rangle_{J=2-5, T=0,1}$ of the MK interaction to build the cross-shell part of the SDPF interaction. The modified MK interaction is exactly the adopted cross-shell interaction of the SDPF-M interaction.

On the basis of the interactions—including the USD, KB, and modified MK interactions—two important modifications are performed: On the one hand, in order to reproduce the unbound property of ^{26}O , modifications are added to the monopole interactions [66]. On the other hand, the pairing matrix elements of the USD interaction are reduced, as it implicitly includes the effects of the pf shell.

The finally obtained SDPF-M was successfully applied to study the exotic properties of the O [44], F [67], Ne [4,16,44], Na [68], Mg [8,44], and Si [44,69] isotopes, such as the unbound structure of $^{26,28}\text{O}$ and the bound structure of $^{32,34}\text{Ne}$. This interaction did well in describing the nuclei with $N \sim 20$, and was used to study the evolution of the $N = 20$ shell gap [44].

2.2. SDPF-MU

The SDPF-MU interaction [53] is based on the USD interaction, the GXPF1B interaction [70], and the V_{MU} interaction [71]. More precisely, its sd -shell part starts from the USD interaction, with the monopole part for the $0d_{3/2}$ and $0d_{5/2}$ orbits modified in the same way as that in the SDPF-M interaction. The GXPF1B interaction is used for the pf -shell part, whereas the TBMEs $\langle 0f_{7/2}0f_{7/2} | V | 0f_{7/2}0f_{7/2} \rangle_{J=0,2}$ are those from the interaction KB3 [72], so as to better describe the nuclei around $N = 22$. Finally, the cross-shell part is composed of the V_{MU} and the M3Y spin-orbit force [73]. To be clearer, V_{MU} is the monopole-based universal force, including the Gaussian central force and the $\pi + \rho$ tensor force. SDPF-MU has been used in the exotic F [3], Mg [55], Si [53,56], and S [53] isotopes [53,56].

2.3. SDPF-U-SI

The SDPF-U/SDPF-U-SI interaction [54] proposed by Nowacki et al. in 2009 is mainly independent of the two interactions mentioned previously. Its proposition aims firstly at nuclei with $8 \leq Z \leq 20$ and $20 \leq N \leq 40$. The model space comprises the full *sd* shell for the protons and the full *pf* shell for the neutrons. Thus, nuclei with around 28 neutrons, along with the neutron excitation across the $N = 28$ shell gap, are the main focus. This is actually based on the SDPF-NR interaction [74,75], which takes the USD interaction, KB' interaction [72], and G-matrix of Kahana, Lee, and Scott [76] as the *sd*-shell interaction, *pf*-shell interaction, and cross-shell interaction, respectively. Iterations are realized to derive the proper monopole changes with the help of the newly discovered experimental data. For instance, after iterations, SDPF-U-SI is able to reproduce the level of the $3/2_1^-$ state of ^{35}Si and the newly discovered spectrum of ^{41}Ca [54].

When applying the three interactions involving the orbits of two major shells, the center-of-mass (c.m.) correction is also considered. This work uses the model of Gloeckner and Lawson [77], which writes the Hamiltonian as $H' = H_{\text{SM}} + \beta_{\text{c.m.}} H_{\text{c.m.}}$ in order to decouple the original Hamiltonian (H_{SM}) and the c.m. Hamiltonian ($H_{\text{c.m.}}$). According to [51], $\beta_{\text{c.m.}} = 10$ is large enough in the calculations of low-lying states, and is used in this work.

In sum, the three interactions are proposed in different ways. The model space of SDPF-MU is the same as that of SDPF-U-SI, while it is larger than that of SDPF-M. Moreover, SDPF-MU and SDPF-U-SI are proposed primarily for nuclei with $N \sim 28$. The two interactions have been compared in the calculations of ^{42}Si . Results showed that CISM calculations with SDPF-MU agreed better with existing data [56]. Nevertheless, in the calculations of nuclei around $N = 20$, the best interaction is not evident. Despite the differences, all of the interactions showed good performance for nuclei in the *sdpf* region. With the three interactions, this paper focuses on the effects of the cross-shell excitation on describing F and Ne nuclei around $N = 20$.

3. Results and Discussions

In this work, we performed CISM calculations to derive the binding energies and energy spectra of F and Ne neutron-rich isotopes. We started with three interactions—SDPF-M, SDPF-MU, and SDPF-U-SI—separately, in order to examine the effects of the cross-shell excitation on the ground-state properties and excitation energies of F and Ne isotopes near $N = 20$. The CISM calculations were carried out in three cases: with cross-shell excitation of the least neutrons (no for positive states and one for negative states, labeled as $(0-1)\hbar\omega$), with cross-shell excitation of at most two neutrons beyond the first case (labeled as $(0-3)\hbar\omega$), and with cross-shell excitation of at most four neutrons beyond the first case (labeled as $(0-5)\hbar\omega$). There are a total of nine groups of theoretical results for all of the involved nuclei.

In this section, the nine groups of ground-state properties and excitation energies are compared with experimental results in order to analyze the contributions of the cross-shell excitation, and then the results of configuration-mixing and occupancy are given to illustrate the analysis; furthermore, the shell structure and evolution described by the three interactions are discussed in order to complete the analysis.

3.1. Ground-State Properties

The foremost task of the theoretical study on F and Ne isotopes around $N = 20$ is to reproduce and explain the location of neutron drip lines by analyzing the separation energies of one neutron (S_n) and two neutrons (S_{2n}). Normally, if the S_n (S_{2n}) of a nucleus is negative, it will be single (double)-neutron(s) unbound. Thus, both the S_n and S_{2n} of a bound nucleus should be positive. In addition, if adding one or two neutrons to a bound nucleus results in unbound nuclei, it can be speculated that such bound nuclei are located in the neutron drip line.

Table 1 shows the theoretical and experimental [14] separation energies of F and Ne nuclei around $N = 20$. For the nuclei with experimental separation energies listed in Table 1, the inclusion of the $(2-3)\hbar\omega$ cross-shell excitation can globally improve the calculation accuracy. Figure 1 illustrates the root-mean-square errors (RMSEs) of the calculated S_n and S_{2n} values of nuclei $^{27-29}\text{F}$ and $^{28-31}\text{Ne}$, compared to experimental data. It can be seen that the RMSEs are smaller after considering the $(2-3)\hbar\omega$ cross-shell excitation. However, the cross-shell excitation part of the SDPF-MU interaction should be improved, as the RMSEs of S_n in the nuclei of $^{27-29}\text{F}$ and $^{28-31}\text{Ne}$ are larger in the $(0-5)\hbar\omega$ case than those in the $(0-3)\hbar\omega$ case.

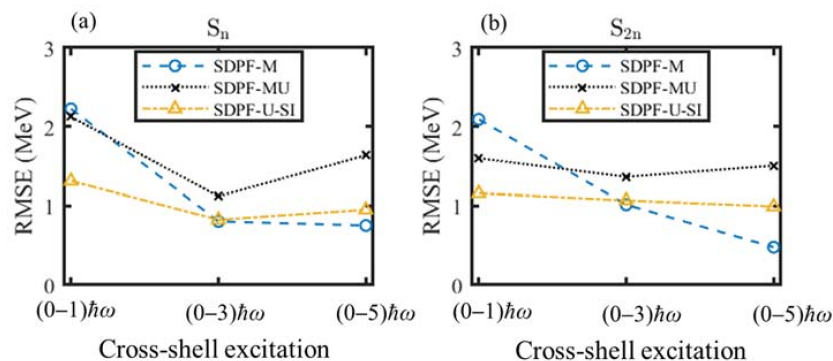


Figure 1. RMSEs of theoretical S_n (a) and S_{2n} (b) values of $^{27-29}\text{F}$ and $^{28-31}\text{Ne}$.

It should be noted that the description improvement of the ground-state properties caused by the cross-shell excitation is rather evident in ^{29}F and ^{30}Ne . The S_n and S_{2n} values of the two nuclei with $N = 20$ are shown in Figure 2. In detail, CISM with the least cross-shell excitation underestimates the energies necessary to separate one or two neutrons from ^{29}F and ^{30}Ne . Then, the inclusion of higher $\hbar\omega$ states leads to the increase in the S_n and S_{2n} values of ^{29}F and ^{30}Ne , typically making the theoretical values closer to the observation results. For instance, in the calculation of S_n (^{29}F) with SDPF-M, the further inclusion of $(2-3)\hbar\omega$ states can take it from negative value to positive value, while that of $(4-5)\hbar\omega$ states allows it to approach the experimental results further. In total, a model space including $(0-5)\hbar\omega$ cross-shell excitation is suggested to sufficiently describe the ground-state properties of ^{29}F and ^{30}Ne within the framework of CISM.

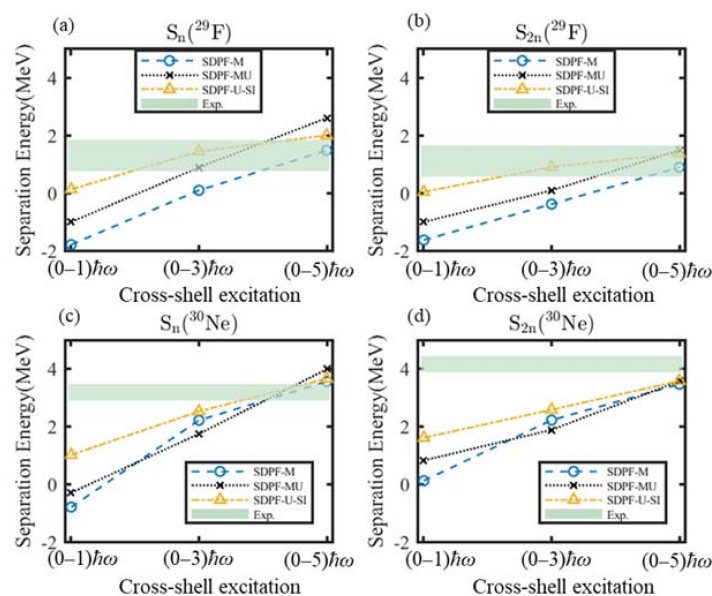


Figure 2. (a) S_n values of ^{29}F , (b) S_{2n} values of ^{29}F , (c) S_n values of ^{30}Ne and (d) S_{2n} values of ^{30}Ne , as calculated by CISM (experimental results are from [14]).

Table 1. The S_n and S_{2n} values (in MeV) of $^{27-33}\text{F}$ and $^{28-36}\text{Ne}$ nuclei calculated by CISM, in comparison with experimental data from the Atomic Mass Evaluation Table 2020 [14].

	Exp. (Error)	SDPF-M (0–1) $\hbar\omega$	SDPF-M (0–3) $\hbar\omega$	SDPF-M (0–5) $\hbar\omega$	SDPF-MU (0–1) $\hbar\omega$	SDPF-MU (0–3) $\hbar\omega$	SDPF-MU (0–5) $\hbar\omega$	SDPF-U-SI (0–1) $\hbar\omega$	SDPF-U-SI (0–3) $\hbar\omega$	SDPF-U-SI (0–5) $\hbar\omega$
S_n (^{27}F)	1.610 (0.060)	0.886	2.437	2.659	1.114	3.200	3.934	2.402	3.027	3.154
S_n (^{28}F)	−0.199 (0.006)	0.157	−0.479	−0.584	0.003	−0.796	−1.113	−0.090	−0.541	−0.622
S_n (^{29}F)	1.320 (0.540)	−1.762	0.116	1.498	−0.980	0.908	2.619	0.152	1.465	2.016
S_n (^{30}F)	/	0.830	−0.799	−1.217	1.075	−1.005	−1.774	0.240	−0.362	−0.652
S_n (^{31}F)	/	−0.502	0.999	1.005	0.117	1.491	1.845	1.325	1.232	1.200
S_n (^{32}F)	/	0.178	−1.423	−1.787	−0.222	−2.015	−2.689	−0.095	−0.860	−1.077
S_n (^{33}F)	/	−0.851	0.535	0.564	−0.140	0.895	1.067	0.537	0.636	0.675
S_n (^{28}Ne)	3.820 (0.160)	2.607	4.477	4.824	2.500	5.328	6.359	4.086	4.861	5.060
S_n (^{29}Ne)	0.970 (0.200)	0.908	0.005	−0.091	1.111	0.137	−0.410	0.592	0.059	−0.081
S_n (^{30}Ne)	3.190 (0.290)	−0.771	2.225	3.562	−0.274	1.757	3.987	1.032	2.532	3.663
S_n (^{31}Ne)	0.170 (0.130)	2.864	0.304	−0.474	3.657	0.998	−1.179	2.441	0.681	−0.478
S_n (^{32}Ne)	/	0.520	2.247	2.352	1.247	2.616	3.763	2.239	2.990	3.319
S_n (^{33}Ne)	/	1.495	−0.969	−1.334	1.598	−1.216	−2.224	0.723	−0.127	−0.446
S_n (^{34}Ne)	/	−0.085	1.483	1.540	0.970	2.315	2.468	2.264	2.173	2.186
S_n (^{35}Ne)	/	0.067	−1.629	−1.902	−1.514	−2.470	−3.016	−0.512	−0.943	−1.032
S_n (^{36}Ne)	/	−0.110	1.156	1.143	0.721	1.211	1.327	0.798	0.822	0.830
S_{2n} (^{27}F)	2.340 (0.150)	1.276	2.746	2.975	2.038	4.307	5.079	3.323	4.217	4.353
S_{2n} (^{28}F)	1.410 (0.060)	1.043	1.958	2.075	1.117	2.404	2.821	2.312	2.486	2.532
S_{2n} (^{29}F)	1.130 (0.540)	−1.605	−0.363	0.914	−0.977	0.112	1.506	0.062	0.924	1.394
S_{2n} (^{30}F)	/	−0.932	−0.683	0.281	0.095	−0.097	0.845	0.392	1.103	1.364
S_{2n} (^{31}F)	/	0.328	0.200	−0.212	1.192	0.486	0.071	1.565	0.870	0.548
S_{2n} (^{32}F)	/	−0.324	−0.424	−0.782	−0.105	−0.524	−0.844	1.230	0.372	0.123
S_{2n} (^{33}F)	/	−0.673	−0.888	−1.223	−0.362	−1.120	−1.622	0.442	−0.224	−0.402
S_{2n} (^{28}Ne)	5.320 (0.130)	3.766	5.367	5.719	4.415	6.404	7.378	5.382	6.183	6.375
S_{2n} (^{29}Ne)	4.790 (0.170)	3.515	4.482	4.733	3.611	5.465	5.949	4.678	4.920	4.979
S_{2n} (^{30}Ne)	4.160 (0.280)	0.137	2.230	3.471	0.837	1.894	3.577	1.624	2.591	3.582
S_{2n} (^{31}Ne)	3.360 (0.310)	2.093	2.529	3.088	3.383	2.755	2.808	3.473	3.213	3.185
S_{2n} (^{32}Ne)	/	3.384	2.551	1.878	4.904	3.614	2.584	4.680	3.671	2.841
S_{2n} (^{33}Ne)	/	2.015	1.278	1.018	2.845	1.400	1.539	2.962	2.863	2.873
S_{2n} (^{34}Ne)	/	1.410	0.514	0.206	2.568	1.099	0.244	2.987	2.046	1.740
S_{2n} (^{35}Ne)	/	−0.018	−0.146	−0.362	−0.544	−0.155	−0.548	1.752	1.230	1.154
S_{2n} (^{36}Ne)	/	−0.043	−0.473	−0.759	−0.793	−1.259	−1.689	0.286	−0.121	−0.202

The qualitative description of the ground states in the nuclei near the F and Ne drip line requires the consideration of the neutron cross-shell excitation beyond the $(0-1)\hbar\omega$ case. Based on the S_n and S_{2n} values, the neutron drip lines are finally determined. In the $(0-1)\hbar\omega$ case, CISM calculations using SDPF-M, SDPF-MU, and SDPF-U-SI predict 28, 31, and 33, respectively, as the largest atomic number of bound F isotopes. However, according to recent experiments, the heaviest bound F isotope is ^{31}F [12]. In the $(0-3)\hbar\omega$ case, both SDPF-M and SDPF-U-SI succeed in reproducing the drip line of F; the results of Ne are rather similar. Only with $(0-1)\hbar\omega$ do CISM calculations with SDPF-M predict an inner drip line of Ne, while those with SDPF-U-SI predict outer. Then, in the case of $(0-3)\hbar\omega$, the results of the two interactions are consistent with the observations. Though SDPF-MU with $(0-1)\hbar\omega$ can reproduce the location of the drip line of F and Ne, it wrongly gives unbound results of ^{29}F and ^{30}Ne , while the neutron cross-shell excitation corrects the descriptions.

Nevertheless, whether or not CISM with $(0-5)\hbar\omega$ can give a significantly better theoretical description of F and Ne chains than that with $(0-3)\hbar\omega$ requires further study. For instance, the three interactions with $(0-5)\hbar\omega$ all incorrectly result in the unbound properties of $^{29,31}\text{Ne}$, while those with $(0-3)\hbar\omega$ do not, which should not happen in principle. Improvements are needed in the cross-shell excitation parts of the three interactions.

The cross-shell excitation is also fundamental to reproducing the ground-state spin of F and Ne nuclei around $N = 20$. Table 2 shows the ground-state spin of $^{27-31}\text{F}$ and $^{28-34}\text{Ne}$, given by experiments or CISM calculations. In the $(0-1)\hbar\omega$ case, the CISM calculation with the SDPF-M interaction cannot reproduce the ground-state spin of ^{28}F and $^{29,31,32}\text{Ne}$, while those with SDPF-MU or with SDPF-U-SI fail, in ^{31}Ne . In the $(0-3)\hbar\omega$ case, the CISM calculation with SDPF-M corrects the ground-state spin of ^{28}F and $^{31,32}\text{Ne}$. Then, in the $(0-5)\hbar\omega$ case, the CISM calculations using the SDPF-MU interaction correct the ground-state spin of ^{31}Ne calculated with $(0-1)\hbar\omega$ and $(0-3)\hbar\omega$. Therefore, the cross-shell excitation is necessary in order to calculate the ground-state spin in F and Ne nuclei around $N = 20$, and more than $(0-3)\hbar\omega$ should be considered. Furthermore, it is suggested that 4^- and $3/2^-$ should be the ground-state spin of ^{30}F and ^{33}Ne , respectively.

Table 2. The experimental and theoretical ground-state spin of $^{27-31}\text{F}$ and $^{28-34}\text{Ne}$ (experimental results are from [78]).

Nucleus	Exp.	SDPF-M (0-1) $\hbar\omega$	SDPF-M (0-3) $\hbar\omega$	SDPF-M (0-5) $\hbar\omega$	SDPF-MU (0-1) $\hbar\omega$	SDPF-MU (0-3) $\hbar\omega$	SDPF-MU (0-5) $\hbar\omega$	SDPF-U-SI (0-1) $\hbar\omega$	SDPF-U-SI (0-3) $\hbar\omega$	SDPF-U-SI (0-5) $\hbar\omega$
^{27}F	$5/2^+$	$5/2^+$	$5/2^+$	$5/2^+$	$5/2^+$	$5/2^+$	$5/2^+$	$5/2^+$	$5/2^+$	$5/2^+$
^{28}F	4^-	6^-	4^-	4^-	4^-	4^-	4^-	4^-	4^-	4^-
^{29}F	$5/2^+$	$5/2^+$	$5/2^+$	$5/2^+$	$5/2^+$	$5/2^+$	$5/2^+$	$5/2^+$	$5/2^+$	$5/2^+$
^{30}F	/	3^+	4^-	4^-	3^+	3^+	4^-	3^+	4^-	4^-
^{31}F	/	$5/2^+$	$5/2^+$	$5/2^+$	$5/2^+$	$5/2^+$	$5/2^+$	$5/2^+$	$5/2^+$	$5/2^+$
^{28}Ne	0^+	0^+	0^+	0^+	0^+	0^+	0^+	0^+	0^+	0^+
^{29}Ne	$3/2^-$	$7/2^-$	$7/2^-$	$3/2^+$	$3/2^-$	$3/2^-$	$3/2^-$	$3/2^-$	$3/2^-$	$3/2^-$
^{30}Ne	0^+	0^+	0^+	0^+	0^+	0^+	0^+	0^+	0^+	0^+
^{31}Ne	$3/2^-$	$3/2^+$	$3/2^-$	$3/2^-$	$3/2^+$	$3/2^+$	$3/2^-$	$3/2^+$	$3/2^+$	$3/2^+$
^{32}Ne	0^+	3^-	0^+	0^+	0^+	0^+	0^+	0^+	0^+	0^+
^{33}Ne	/	$3/2^+$	$3/2^-$	$3/2^-$	$3/2^+$	$3/2^+$	$3/2^-$	$3/2^-$	$3/2^-$	$3/2^-$
^{34}Ne	/	0^+	0^+	0^+	0^+	0^+	0^+	0^+	0^+	0^+

In total, the cross-shell excitation is crucial to describing the ground states of F and Ne isotopes around $N = 20$. Furthermore, $(0-5)\hbar\omega$ excitation could be necessary to the ^{29}F and ^{30}Ne nuclei. The cross-shell excitation parts of the three interactions may not be well fixed yet.

3.2. Excitation Energies

Since many of the F and Ne nuclei around $N = 20$ are weakly bound, the experimental results of the excited states are rather rare. To date, there is no information about the excited

states of the F (Ne) isotopes heavier than 29 (32) in the Nudat2 database [79]. Therefore, this paper focused on selected low-lying states. Table 3 shows the experimental and theoretical energy levels of the excited states in F and Ne nuclei around $N = 20$.

Table 3. The experimental and theoretical energy levels (in MeV) of the excited state in F and Ne nuclei (the experimental results are from [79], except those for $^{27,29}\text{F}$, which are from [67]).

Nucleus	State	Exp.	SDPF-M (0–1) $\hbar\omega$	SDPF-M (0–3) $\hbar\omega$	SDPF-M (0–5) $\hbar\omega$	SDPF-MU (0–1) $\hbar\omega$	SDPF-MU (0–3) $\hbar\omega$	SDPF-MU (0–5) $\hbar\omega$	SDPF-U-SI (0–1) $\hbar\omega$	SDPF-U-SI (0–3) $\hbar\omega$	SDPF-U-SI (0–5) $\hbar\omega$
^{27}F	$1/2_1^+$	0.915 (0.012)	1.980	1.297	1.184	2.176	1.952	1.482	1.923	1.770	1.715
	$3/2_1^+$	/	2.626	2.732	2.675	2.847	3.571	3.452	2.872	3.218	3.293
^{29}F	$1/2_1^+$	1.080 (0.018)	3.553	0.952	0.797	3.669	2.833	1.515	2.736	2.116	1.294
	$3/2_1^+$	/	6.407	2.246	2.294	6.349	5.047	3.442	6.660	3.829	2.816
^{31}F	$1/2_1^+$	/	0.648	0.542	0.628	0.311	0.680	0.796	0.176	0.340	0.390
	$3/2_1^+$	/	1.868	1.701	2.019	1.821	2.342	2.618	1.447	1.681	1.764
^{28}Ne	2_1^+	1.304 (0.003)	1.553	1.401	1.362	1.830	2.110	2.196	1.804	1.947	1.983
	4_1^+	3.010 (0.006)	2.952	2.770	2.757	3.302	3.512	3.779	3.342	3.458	3.510
^{30}Ne	2_1^+	0.792 (0.004)	1.531	0.873	1.028	1.912	1.997	1.808	1.901	1.760	1.201
	4_1^+	2.235 (0.012)	2.444	1.945	2.364	2.817	2.954	3.359	2.879	2.935	2.535
^{32}Ne	2_1^+	0.722 (0.009)	0.768	0.682	0.841	0.857	1.262	1.482	0.659	0.858	0.932
	4_1^+	/	1.763	1.778	2.086	2.120	2.784	3.253	1.762	2.092	2.241
^{34}Ne	2_1^+	/	0.521	0.838	0.969	0.690	1.110	1.403	0.476	0.616	0.655
	4_1^+	/	1.387	2.028	2.267	1.922	2.670	3.158	1.424	1.679	1.747

For F isotopes, the odd- A nuclei are our first focused. According to the shell model, such nuclei should have a $5/2^+$ ground state caused by a valence proton on the $\pi 0d_{5/2}$ orbit. When the valence proton moves to the $\pi 1s_{1/2}$ ($\pi 0d_{3/2}$) orbit, the spin of the excited states should be $1/2^+$ ($3/2^+$). Although a state is rarely a pure, single-particle state in the view of CISM, the order $5/2^+$, $1/2^+$, and $3/2^+$ holds. This is because the $\pi 0d_{5/2}$ configuration dominates on the $5/2^+$ ground state, and similar explanations work for the other cases.

In all cases discussed in this paper, the theoretical ground-state spins of odd- A F isotopes are $5/2^+$. For the first $1/2^+$ state, the cross-shell excitation is shown to be necessary to the CISM calculation. It can be seen from Table 3 that the theoretical energy levels of $1/2_1^+$ of $^{27,29}\text{F}$ are much higher than the existing experimental levels. From $(0-1)\hbar\omega$ to $(0-3)\hbar\omega$, those energy levels become lower; then, from $(0-3)\hbar\omega$ to $(0-5)\hbar\omega$, they decrease again. It can be noted that the latter decreases are less significant than the former. Overall, the inclusion of cross-shell excitation beyond the $(0-1)\hbar\omega$ states makes the theoretical levels of the $1/2_1^+$ of odd- A $^{27,29}\text{F}$ approach the experimental results significantly. Considering the experimental errors and the possible deficiency of the interactions involved, it is suggested that $(0-3)\hbar\omega$ is insufficient to reproduce those $1/2_1^+$ states. In particular, the results of the $1/2_1^+$ state in ^{29}F are illustrated in Figure 3; according to this figure, the necessity of $(0-5)\hbar\omega$ is indicated in the interpretation of the energy spectrum of ^{29}F .

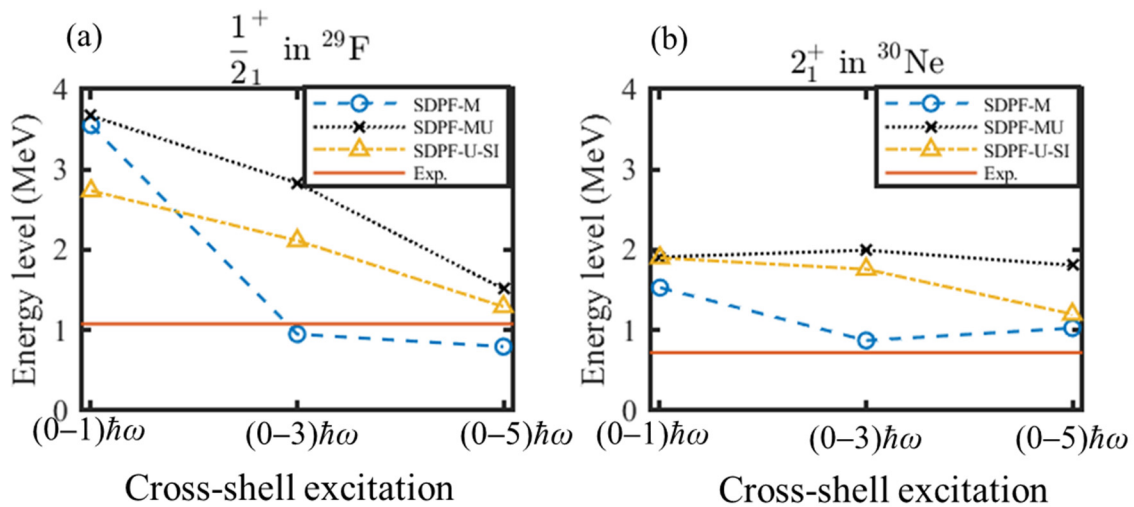


Figure 3. The energy levels of (a) the $1/2_1^+$ state in ^{29}F and (b) the 2_1^+ state in ^{30}Ne , calculated by the CISM (experimental data are from [67] (a) and Nudat2 (b)).

Theoretically, the three lowest lying states of even-mass Ne isotopes should be 0^+ , 2^+ , and 4^+ by orders. The CISM with SDPF-M wrongly gives 3^- as the ground-state spin in the $(0-1)\hbar\omega$ case, and corrects the result with $(0-3)\hbar\omega$. The levels of the 2_1^+ and 4_1^+ states in even- A $^{28-32}\text{Ne}$ can be seen in Table 3. CISM calculations of these levels with the three interactions are consistent with experimental results. It can be seen that the SDPF-M interaction reasonably reproduces these levels, with RMSE values less than 0.4 MeV. The levels of the 2_1^+ state in ^{30}Ne are also presented in Figure 3. Including higher $\hbar\omega$ states results in slight variations in the energy spectra of ^{28}Ne , while the inclusion of $(2-3)\hbar\omega$ states helps SDPF-M to better describe the 2_1^+ state in ^{30}Ne . For SDPF-U-SI, theoretical results with $(0-5)\hbar\omega$ are the most consistent with the experimental results, both for the 2_1^+ state in ^{30}Ne , and for the overall levels in even- A $^{28-32}\text{Ne}$. However, it should also be noted that the global description accuracy of levels of SDPU-MU deteriorates with the enlargement of the model space. In sum, it is believed that the cross-shell excitation plays an important role in CISM calculations of Ne isotopes around $N = 20$.

The level of the first intruder state is also of interest. It was found that the levels of the first negative state of odd- A $^{27-31}\text{F}$ and even- A $^{28-34}\text{Ne}$ increase with the addition of $\hbar\omega$. Moreover, the level variation is more significant from the $(0-1)\hbar\omega$ case to the $(0-3)\hbar\omega$ case than from the $(0-3)\hbar\omega$ case to the $(0-5)\hbar\omega$ case.

Overall, the cross-shell excitation is necessary to well describe the excited states of F and Ne nuclei around $N = 20$, and it is suggested to consider $(0-5)\hbar\omega$ in the calculations of ^{29}F and ^{30}Ne .

3.3. Configuration Occupancies

From Sections 3.1 and 3.2, it is known that the cross-shell excitation is crucial to describe F and Ne nuclei around $N = 20$ within the CISM framework. This means that the $N = 20$ shell gap is reduced or vanished, and neutrons occupy the pf -shell orbits. This phenomenon can be illustrated with the configuration occupancy.

Table 4 shows the average neutrons that occupy the pf -shell orbits in the odd-F and even-Ne isotopes. For the $N = 18$ nuclei, there are large possibilities of neutron excitation across the $N = 20$ shell gap; thus, the interactions without cross-shell excitation are insufficient to reproduce the ground-state properties of ^{27}F and ^{28}Ne . Similar explanations can be found in the nuclei with $N = 22$ or 24. Thus, the overall description of the ground states in F and Ne nuclei near the neutron drip lines—including the determination of the neutron drip lines—requires the cross-shell excitation.

Table 4. The average neutron occupancies of F and Ne nuclei in the pf shell with $N \sim 20$.

Nucleus	State	(0–1) $\hbar\omega$	(0–3) $\hbar\omega$ SDPF-M	(0–3) $\hbar\omega$ SDPF-MU	(0–3) $\hbar\omega$ SDPF-U-SI	(0–5) $\hbar\omega$ SDPF-M	(0–5) $\hbar\omega$ SDPF-MU	(0–5) $\hbar\omega$ SDPF-U-SI
^{27}F	$5/2_1^+$	0	0.795	0.543	0.236	0.951	0.877	0.300
^{29}F	$5/2_1^+$	0	1.497	0.646	0.457	2.354	1.660	0.930
^{29}F	$1/2_1^+$	0	1.972	1.003	1.226	2.716	2.302	1.967
^{29}F	$3/2_1^+$	0	1.994	1.356	1.971	2.730	2.330	2.127
^{31}F	$5/2_1^+$	2	3.413	2.689	2.346	4.030	3.452	2.519
^{33}F	$5/2_1^+$	4	5.337	4.669	4.234	5.745	5.214	4.298
^{28}Ne	0_1^+	0	1.090	0.570	0.261	1.307	1.089	0.377
^{30}Ne	0_1^+	0	1.857	0.700	0.669	2.479	1.958	1.619
^{30}Ne	2_1^+	0	1.965	0.690	1.330	2.533	2.192	2.053
^{30}Ne	4_1^+	0	1.981	0.589	1.016	2.404	1.953	2.050
^{32}Ne	0_1^+	2	3.705	2.693	2.385	4.038	3.515	2.660
^{34}Ne	0_1^+	4	5.344	4.566	4.204	5.654	5.101	4.268

Among the nuclei investigated in this paper, ^{29}F and ^{30}Ne are the most special, as the sd shell is fully occupied, without cross-shell excitation. However, results in a larger model space show that neutrons in ^{29}F and ^{30}Ne occupy the pf -shell orbits. CISM calculations using the SDPF-M interaction with the (0–5) $\hbar\omega$ case indicate that more than two neutrons in ^{29}F and ^{30}Ne excite across the $N = 20$ shell gap on average. This explains the necessity of a model space including (0–5) $\hbar\omega$ excitation in describing ^{29}F and ^{30}Ne .

In detail, Table 5 gives the configuration occupancies of the ground states in ^{29}F and ^{30}Ne . In the (0–1) $\hbar\omega$ case, ^{29}F and ^{30}Ne are pure $\pi 0d_{5/2} \nu(0d_{3/2})^4$ and $\pi(0d_{5/2})^2 \nu(0d_{3/2})^4$ configurations, respectively. However, results considering the cross-shell excitation show that the $\pi 0d_{5/2} \nu(0d_{3/2})^2 (0f_{7/2})^2$ configuration is strongly mixed with $\pi 0d_{5/2} \nu(0d_{3/2})^4$ in ^{29}F . CISM calculations with SDPF-M indicate that the $\pi 0d_{5/2} \nu(0d_{3/2})^2 (0f_{7/2})^2$ configuration is actually dominant in the ground state of ^{29}F . In such a configuration, two neutrons of ^{29}F (^{30}Ne also) excite from the $\nu 0d_{3/2}$ orbit to the $\nu 0f_{7/2}$ orbit. The configurations $\pi 0d_{5/2} \nu(0d_{3/2})^2 (1p_{3/2})^2$ and $\pi(0d_{5/2})^2 \nu(0d_{3/2})^2 (1p_{3/2})^2$, which represent the excitation of a pair of neutrons to the $\nu 1p_{3/2}$ orbit, are also important in ^{29}F and ^{30}Ne , respectively. Therefore, it is necessary to consider the three kinds of configurations in ^{29}F and ^{30}Ne .

Table 5. Percentages (in %) of the configurations in the ground states.

Nucleus	Configuration	(0–1) $\hbar\omega$	(0–3) $\hbar\omega$ SDPF-M	(0–3) $\hbar\omega$ SDPF-MU	(0–3) $\hbar\omega$ SDPF-U-SI	(0–5) $\hbar\omega$ SDPF-M	(0–5) $\hbar\omega$ SDPF-MU	(0–5) $\hbar\omega$ SDPF-U-SI
^{29}F	$\pi 0d_{5/2} \nu(0d_{3/2})^4$	1	24.98	65.81	76.24	8.53	30.65	56.14
	$\pi 0d_{5/2} \nu(0d_{3/2})^2 (0f_{7/2})^2$	0	43.65	13.83	9.53	36.16	20.56	15.91
	$\pi 0d_{5/2} \nu(0d_{3/2})^2 (1p_{3/2})^2$	0	15.41	4.42	2.93	15.14	14.28	7.92
^{30}Ne	$\pi(0d_{5/2})^2 \nu(0d_{3/2})^4$	1	6.55	57.88	59.73	2.98	17.45	22.58
	$\pi(0d_{5/2})^2 \nu(0d_{3/2})^2 (0f_{7/2})^2$	0	45.4	12.88	11.08	32.53	17.94	17.49
	$\pi(0d_{5/2})^2 \nu(0d_{3/2})^2 (1p_{3/2})^2$	0	10.27	3.41	3.74	8.56	10.33	10.21

In conclusion, neutrons of F and Ne nuclei excite from sd -shell orbits to pf -shell orbits when the neutron number approaches 20. This phenomenon makes it necessary for F and Ne nuclei around $N = 20$ to include the cross-shell excitation. Taking ^{29}F and ^{30}Ne , for example, in both the ground state and excited states, the neutrons exciting to the pf -shell are in significant numbers, which explains why CISM calculations with (0–1) $\hbar\omega$ or (0–3) $\hbar\omega$ fail in describing ^{29}F and ^{30}Ne .

3.4. Shell Structure and Evolution

This section tries to explain why some CISM calculations, including $(4-5)\hbar\omega$ states, are less consistent with experimental results. The shell structure and its evolution are compared among the three interactions via their effective single-particle energies (ESPEs) [80,81] and a monopole-frozen analysis [82].

For an orbit j , the ESPE can be expressed as [80,81]:

$$\varepsilon_j = \varepsilon_j^{core} + \sum_{j'} V_{jj'} \langle \psi | \hat{N}_{j'} | \psi \rangle \quad (1)$$

where ε_j^{core} represents the SPE of the j orbit regarding the inert core, $V_{jj'}$ represents the monopole interaction [66] between the j and j' orbits, and $\langle \psi | \hat{N}_{j'} | \psi \rangle$ is the occupancy number of particles in the j' orbit. The monopole interactions are derived from the average of the diagonal TBMEs. In detail, $V_{jj'}$ for a given isospin T is defined as:

$$V_{jj',T} = \sum_J \left[1 - (-1)^{(2j-J-T+1)} \delta(jj') \right] \frac{2J+1}{(2j+1)(2j'+1)} \langle jj' | V | jj' \rangle_{JT} \quad (2)$$

with J as the angular momentum and δ as Kronecker's delta. When valence particles are added to orbits, the monopole interactions will change the SPEs.

To illustrate the shell evolution due to the addition of neutrons, Figure 4 shows the ESPEs in the ground states of Ne isotopes (the results of F isotopes are fairly similar), derived using the three interactions in the $(0-5)\hbar\omega$ model space. It can be deduced that the three interactions give different interpretations of the shell structure and evolution. Firstly, the SDPF-M interaction indicates a rather strong mixing of the three orbits $\nu 0d_{3/2}$, $\nu 1p_{3/2}$, and $\nu 0f_{7/2}$, while $\nu 1p_{3/2}$, $\nu 1p_{1/2}$, and $\nu 0f_{7/2}$ orbits are strongly mixed in the other two interactions. With the increase in mass number, the relative position of $\nu 0f_{7/2}$ ($\nu 1p_{3/2}$) to $\nu 1p_{1/2}$ varies more slowly in SDPF-MU than in SDPF-U-SI. Such differences in shell structure suggest the necessity of improvements in the cross-shell interactions of at least two among the three interactions.

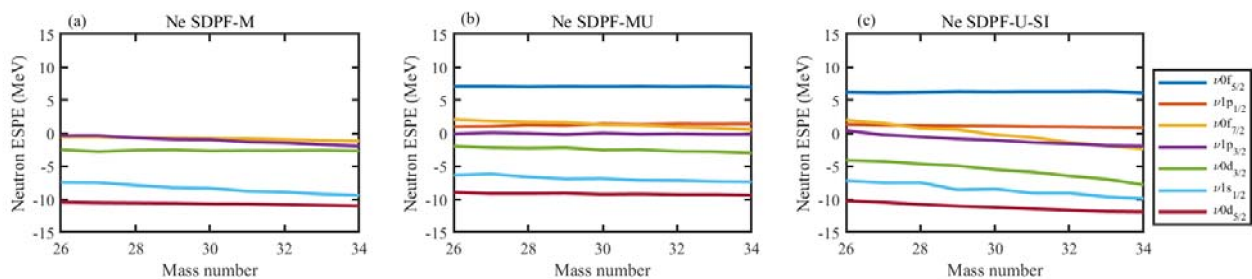


Figure 4. ESPEs in the ground state of Ne isotopes calculated in the $(0-5)\hbar\omega$ model space, with SDPF-M (a), SDPF-MU (b), and SDPF-U-SI (c).

For a given nucleus, the shell evolution can also result from the excitation of valence particles [35,83], which is called the type II shell evolution [83]. We employed monopole-frozen analysis to examine the effects of such shell evolution, as described by the three interactions. In detail, we substituted ESPEs for SPEs, removed the monopole interaction from the diagonal TBMEs, and performed CISM calculations for ^{29}F and ^{30}Ne in the $(0-5)\hbar\omega$ model space. If the type II shell evolution is not significant in the two nuclei, their excitation energies should not be significantly changed by the monopole-frozen calculations.

Figure 5 presents the energy spectra of the two nuclei derived before and after the monopole-frozen modification. Despite the distinct energy spectra, it can be seen that the monopole-frozen modification generates different effects on the selected states for different interactions. For instance, positive yrast states of ^{29}F and ^{30}Ne from all three interactions

change little with monopole-frozen calculations, which means that they share similar shell structures to the ground states. After monopole-frozen modification, the negative states of ^{30}Ne from SDPF-MU and SDPF-U-SI interactions and the second 0^+ state of ^{30}Ne from SDPF-M have changed a lot. Therefore, the three interactions provide different illustrations of the excitation of the ground state for both ^{29}F and ^{30}Ne . Furthermore, a more reliable and effective interaction to describe $N\sim 20$ nuclei with extreme proton–neutron asymmetry is required.

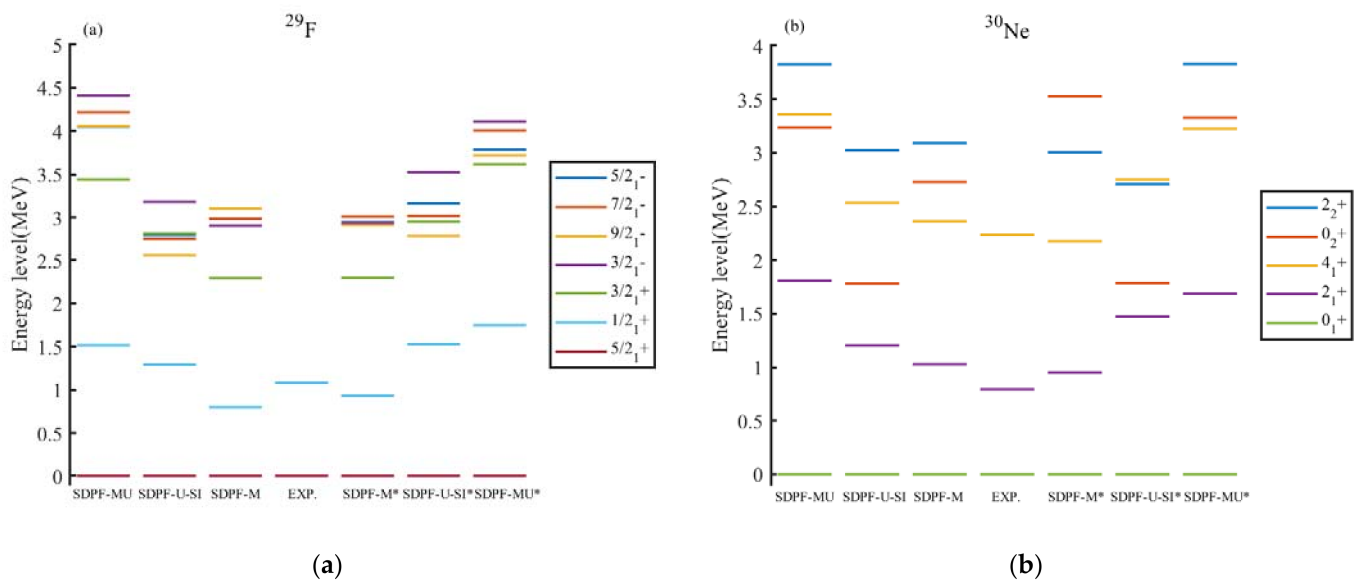


Figure 5. Comparison of energy spectra of (a) ^{29}F and (b) ^{30}Ne . All CISM calculations were performed in the $(0-5)\hbar\omega$ model space. The symbol * represents where the interaction is modified via frozen monopole.

The ESPEs and monopole-frozen effects of the three interactions provide various shell structures and evolutions for F and Ne nuclei near $N = 20$, indicating that they can hardly be consistent with one another. Therefore, the cross-shell parts of the three interactions are suggested to be improved in order to describe the neutron-rich nuclei with $N\sim 20$ better.

4. Conclusions

In this work, three interactions—SDPF-M, SDPF-MU, and SDPF-U-SI—were applied to calculate the structure of neutron-rich F and Ne isotopes within the framework of the configuration–interaction shell model. This paper focused on the cross-shell excitation of F and Ne nuclei near $N = 20$, which are among the systems with the most proton–neutron asymmetry. As a result, the cross-shell excitation was shown to be necessary for the overall description of F and Ne isotopes around $N = 20$. For ^{29}F and ^{30}Ne , it is important to include the cross-shell excitation of $(0-5)\hbar\omega$. Considering the insufficiency of the three interactions in the $(0-5)\hbar\omega$ model space to reproduce properties such as the bound structure of $^{29,31}\text{Ne}$, it is also suggested to optimize the three interactions in order to better describe the cross-shell excitation near ^{29}F and ^{30}Ne in future works. This conclusion is supported by the investigation of ESPEs and a monopole-frozen analysis, which indicate the different illustrations of the three interactions on the shell structure and evolution in the target nuclear region.

Author Contributions: Conceptualization, C.Y.; methodology, C.Y. and M.L.; investigation, C.Y. and M.L.; data curation, C.Y. and M.L.; writing—original draft preparation, M.L.; writing—review and editing, C.Y. and M.L.; supervision, C.Y.; project administration, C.Y.; funding acquisition, C.Y. All authors have read and agreed to the published version of the manuscript.

Funding: This research was funded by the National Natural Science Foundation of China under Grant No. 11775316 and 11305272, the computational resources from SYSU, the National Supercomputer Center in Guangzhou, and the Key Laboratory of High-Precision Nuclear Spectroscopy, Institute of Modern Physics, Chinese Academy of Sciences.

Institutional Review Board Statement: Not applicable.

Informed Consent Statement: Not applicable.

Data Availability Statement: Data is contained within the article.

Acknowledgments: The authors appreciate fruitful discussions from Takaharu Otsuka, Noritaka Shimizu, and Xinxing Xu.

Conflicts of Interest: The authors declare no conflict of interest.

References

- Haxel, O.; Jensen, J.H.D.; Suess, H.E. On the “magic numbers” in nuclear structure. *Phys. Rev.* **1949**, *75*, 1766. [[CrossRef](#)]
- Mayer, M.G. On closed shells in nuclei. II. *Phys. Rev.* **1949**, *75*, 1969–1970. [[CrossRef](#)]
- Revel, A.; Sorlin, O.; Marques, F.M.; Kondo, Y.; Kahlbow, J.; Nakamura, T.; Orr, N.A.; Nowacki, F.; Tostevin, J.A.; Yuan, C.X.; et al. Extending the southern shore of the island of inversion to ^{28}F . *Phys. Rev. Lett.* **2020**, *124*, 152502. [[CrossRef](#)] [[PubMed](#)]
- Terry, J.R.; Bazin, D.; Brown, B.A.; Campbell, C.M.; Church, J.A.; Cook, J.M.; Davies, A.D.; Dinca, D.C.; Enders, J.; Gade, A.; et al. Direct evidence for the onset of intruder configurations in neutron-rich Ne isotopes. *Phys. Lett. B* **2006**, *640*, 86–90. [[CrossRef](#)]
- Dombradi, Z.; Elekes, Z.; Saito, A.; Aoi, N.; Baba, H.; Demichi, K.; Fulop, Z.; Gibelin, J.; Gomi, T.; Hasegawa, H.; et al. Vanishing $N = 20$ shell gap: Study of excited states in $^{27,28}\text{Ne}$. *Phys. Rev. Lett.* **2006**, *96*, 182501. [[CrossRef](#)]
- Liu, H.; Lee, J.; Doornenbal, P.; Scheit, H.; Takeuchi, S.; Aoi, N.; Li, K.; Matsushita, M.; Steppenbeck, D.; Wang, H.; et al. Single-neutron knockout reaction from ^{30}Ne . *JPS Conf. Proc.* **2015**, *6*, 030003.
- Thibault, C.; Klapisch, R.; Rigaud, C.; Poskanzer, A.M.; Prieels, R.; Lessard, L.; Reisdorf, W. Direct measurement of the masses of ^{11}Li and $^{26-32}\text{Na}$ with an on-line mass spectrometer. *Phys. Rev. C* **1975**, *12*, 644–657. [[CrossRef](#)]
- Terry, J.R.; Brown, B.A.; Campbell, C.M.; Cook, J.M.; Davies, A.D.; Dinca, D.C.; Gade, A.; Glasmacher, T.; Hansen, P.G.; Sherrill, B.M.; et al. Single-neutron knockout from intermediate energy beams of $^{30,32}\text{Mg}$: Mapping the transition into the “island of inversion”. *Phys. Rev. C* **2008**, *77*, 014316. [[CrossRef](#)]
- Guillemaud-Mueller, D.; Jacmart, J.C.; Kashy, E.; Latimier, A.; Mueller, A.C.; Pougheon, F.; Richard, A.; Penionzhkevich, Y.E.; Artuhk, A.G.; Belozyorov, A.V.; et al. Particle stability of the isotopes ^{26}O and ^{32}Ne in the reaction $44\text{ MeV/nucleon }^{48}\text{Ca} + \text{Ta}$. *Phys. Rev. C Nucl. Phys.* **1990**, *41*, 937–941. [[CrossRef](#)]
- Tarasov, O.; Allatt, R.; Angélique, J.C.; Anne, R.; Borcea, C.; Dlouhy, Z.; Donzau, C.; Grévy, S.; Guillemaud-Mueller, D.; Lewitowicz, M.; et al. Search for ^{28}O and study of neutron-rich nuclei near the $N = 20$ shell closure. *Phys. Lett. B* **1997**, *409*, 64–70. [[CrossRef](#)]
- Thoennessen, M. Reaching the limits of nuclear stability. *Rep. Prog. Phys.* **2004**, *67*, 1187–1232. [[CrossRef](#)]
- Ahn, D.S.; Fukuda, N.; Geissel, H.; Inabe, N.; Iwasa, N.; Kubo, T.; Kusaka, K.; Morrissey, D.J.; Murai, D.; Nakamura, T.; et al. Location of the neutron dripline at fluorine and neon. *Phys. Rev. Lett.* **2019**, *123*, 212501. [[CrossRef](#)]
- Sakurai, H.; Lukyanov, S.M.; Notani, M.; Aoi, N.; Beaumel, D.; Fukuda, N.; Hirai, M.; Ideguchi, E.; Imai, N.; Ishihara, M.; et al. Evidence for particle stability of F and particle instability of N and O. *Phys. Lett. B* **1999**, *448*, 180–184. [[CrossRef](#)]
- Wang, M.; Huang, W.J.; Kondev, F.G.; Audi, G.; Naimi, S. The AME 2020 atomic mass evaluation (II). Tables, graphs and references*. *Chin. Phys. C* **2021**, *45*, 030003. [[CrossRef](#)]
- Kobayashi, N.; Nakamura, T.; Kondo, Y.; Tostevin, J.A.; Aoi, N.; Baba, H.; Barthelemy, R.; Famiano, M.A.; Fukuda, N.; Inabe, N.; et al. One-neutron removal from ^{29}Ne : Defining the lower limits of the island of inversion. *Phys. Rev. C* **2016**, *93*, 014613. [[CrossRef](#)]
- Nakamura, T.; Kobayashi, N.; Kondo, Y.; Satou, Y.; Aoi, N.; Baba, H.; Deguchi, S.; Fukuda, N.; Gibelin, J.; Inabe, N.; et al. Halo structure of the island of inversion nucleus ^{31}Ne . *Phys. Rev. Lett.* **2009**, *103*, 262501. [[CrossRef](#)]
- Gaudefroy, L.; Mittig, W.; Orr, N.A.; Varet, S.; Chartier, M.; Roussel-Chomaz, P.; Ebran, J.P.; Fernandez-Dominguez, B.; Fremont, G.; Gangnant, P.; et al. Direct mass measurements of ^{19}B , ^{22}C , ^{29}F , ^{31}Ne , ^{34}Na and other light exotic nuclei. *Phys. Rev. Lett.* **2012**, *109*, 202503. [[CrossRef](#)]
- Bagchi, S.; Kanungo, R.; Tanaka, Y.K.; Geissel, H.; Doornenbal, P.; Horiuchi, W.; Hagen, G.; Suzuki, T.; Tsunoda, N.; Ahn, D.S.; et al. Two-Neutron Halo is Unveiled in ^{29}F . *Phys. Rev. Lett.* **2020**, *124*, 222504. [[CrossRef](#)]
- Chrisman, D.; Kuchera, A.N.; Baumann, T.; Blake, A.; Brown, B.A.; Brown, J.; Cochran, C.; DeYoung, P.A.; Finck, J.E.; Frank, N.; et al. Neutron-unbound states in ^{31}Ne . *Phys. Rev. C* **2021**, *104*, 034313. [[CrossRef](#)]
- Jansen, G.R.; Engel, J.; Hagen, G.; Navratil, P.; Signoracci, A. Ab initio coupled-cluster effective interactions for the shell model: Application to neutron-rich oxygen and carbon isotopes. *Phys. Rev. Lett.* **2014**, *113*, 142502. [[CrossRef](#)]
- Sun, Z.; Wu, Q.; Xu, F. Green’s function calculations of light nuclei. *Sci. China Phys. Mech.* **2016**, *59*, 692013. [[CrossRef](#)]

22. Bender, M.; Heenen, P.-H.; Reinhard, P.-G. Self-consistent mean-field models for nuclear structure. *Rev. Mod. Phys.* **2003**, *75*, 121–180. [[CrossRef](#)]
23. Otsuka, T.; Honma, M.; Mizusaki, T.; Shimizu, N.; Utsuno, Y. Monte Carlo shell model for atomic nuclei. *Prog. Part. Nucl. Phys.* **2001**, *47*, 319–400. [[CrossRef](#)]
24. Miyagi, T.; Stroberg, S.R.; Holt, J.D.; Shimizu, N. Ab initio multishell valence-space Hamiltonians and the island of inversion. *Phys. Rev. C* **2020**, *102*, 034320. [[CrossRef](#)]
25. Luo, Y.-X.; Fosse, K.; Liu, Q.; Guo, J.-Y. Role of quadrupole deformation and continuum effects in the “island of inversion” nuclei F28,29,31. *Phys. Rev. C* **2021**, *104*, 014307. [[CrossRef](#)]
26. Tripathi, V.; Tabor, S.L.; Mantica, P.F.; Utsuno, Y.; Bender, P.; Cook, J.; Hoffman, C.R.; Lee, S.; Otsuka, T.; Pereira, J.; et al. Competition between normal and intruder states inside the “island of inversion”. *Phys. Rev. C* **2007**, *76*, 021301. [[CrossRef](#)]
27. Michel, N.; Li, J.G.; Xu, F.R.; Zuo, W. Two-neutron halo structure of ^{31}F . *Phys. Rev. C* **2020**, *101*, 031301. [[CrossRef](#)]
28. Masui, H.; Horiuchi, W.; Kimura, M. Two-neutron halo structure of ^{31}F and a novel pairing antihalo effect. *Phys. Rev. C* **2020**, *101*, 041303. [[CrossRef](#)]
29. Singh, J.; Casal, J.; Horiuchi, W.; Fortunato, L.; Vitturi, A. Exploring two-neutron halo formation in the ground state of ^{29}F within a three-body model. *Phys. Rev. C* **2020**, *101*, 024310. [[CrossRef](#)]
30. Lee, J.; Xu, X.X.; Kaneko, K.; Sun, Y.; Lin, C.J.; Sun, L.J.; Liang, P.F.; Li, Z.H.; Li, J.; Wu, H.Y.; et al. Large isospin asymmetry in $^{22}\text{Si}/^{22}\text{O}$ mirror Gamow-Teller transitions reveals the halo structure of ^{22}Al . *Phys. Rev. Lett.* **2020**, *125*, 192503. [[CrossRef](#)]
31. Liang, P.F.; Sun, L.J.; Lee, J.; Hou, S.Q.; Xu, X.X.; Lin, C.J.; Yuan, C.X.; He, J.J.; Li, Z.H.; Wang, J.S.; et al. Simultaneous measurement of β -delayed proton and γ emission of ^{26}P for the $^{25}\text{Al}(p,\gamma)^{26}\text{Si}$ reaction rate. *Phys. Rev. C* **2020**, *101*, 024305. [[CrossRef](#)]
32. Sun, L.J.; Xu, X.X.; Hou, S.Q.; Lin, C.J.; José, J.; Lee, J.; He, J.J.; Li, Z.H.; Wang, J.S.; Yuan, C.X.; et al. Experimentally well-constrained masses of ^{27}P and ^{27}S : Implications for studies of explosive binary systems. *Phys. Lett. B* **2020**, *802*, 135213. [[CrossRef](#)]
33. Shi, G.Z.; Liu, J.J.; Lin, Z.Y.; Zhu, H.F.; Xu, X.X.; Sun, L.J.; Liang, P.F.; Lin, C.J.; Lee, J.; Yuan, C.X.; et al. β -delayed two-proton decay of ^{27}S at the proton-drip line. *Phys. Rev. C* **2021**, *103*, L061301. [[CrossRef](#)]
34. Chen, Z.Q.; Li, Z.H.; Hua, H.; Watanabe, H.; Yuan, C.X.; Zhang, S.Q.; Lorusso, G.; Nishimura, S.; Baba, H.; Browne, F.; et al. Proton shell evolution below ^{132}Sn : First measurement of low-lying beta-emitting isomers in $^{123,125}\text{Ag}$. *Phys. Rev. Lett.* **2019**, *122*, 212502. [[CrossRef](#)]
35. Xu, X.; Liu, J.H.; Yuan, C.X.; Xing, Y.M.; Wang, M.; Zhang, Y.H.; Zhou, X.H.; Litvinov, Y.A.; Blaum, K.; Chen, R.J.; et al. Masses of ground and isomeric states of ^{101}In and configuration-dependent shell evolution in odd-A indium isotopes. *Phys. Rev. C* **2019**, *100*, 051303. [[CrossRef](#)]
36. Yuan, C.X.; Liu, Z.; Xu, F.R.; Walker, P.M.; Podolyák, Z.; Xu, C.; Ren, Z.Z.; Ding, B.; Liu, M.L.; Liu, X.Y.; et al. Isomerism in the “south-east” of ^{132}Sn and a predicted neutron-decaying isomer in ^{129}Pd . *Phys. Lett. B* **2016**, *762*, 237–242. [[CrossRef](#)]
37. Phong, V.H.; Lorusso, G.; Davinson, T.; Estrade, A.; Hall, O.; Liu, J.; Matsui, K.; Montes, F.; Nishimura, S.; Boso, A.; et al. Observation of a μs isomer in ^{134}In : Proton-neutron coupling “southeast” of ^{132}Sn . *Phys. Rev. C* **2019**, *100*, 011302. [[CrossRef](#)]
38. Li, C.B.; Zhang, G.L.; Yuan, C.X.; Zhang, G.X.; Hu, S.P.; Qu, W.W.; Zheng, Y.; Zhang, H.Q.; Mengoni, D.; Testov, D.; et al. New level scheme and shell model description of ^{212}Rn . *Phys. Rev. C* **2020**, *101*, 044313. [[CrossRef](#)]
39. Zhang, M.M.; Yang, H.B.; Gan, Z.G.; Zhang, Z.Y.; Huang, M.H.; Ma, L.; Yang, C.L.; Yuan, C.X.; Wang, Y.S.; Tian, Y.L.; et al. A new isomeric state in ^{218}Pa . *Phys. Lett. B* **2020**, *800*, 135102. [[CrossRef](#)]
40. Zhou, H.B.; Gan, Z.G.; Wang, N.; Yang, H.B.; Ma, L.; Huang, M.H.; Yang, C.L.; Zhang, M.M.; Tian, Y.L.; Wang, Y.S.; et al. Lifetime measurement for the isomeric state in ^{213}Th . *Phys. Rev. C* **2021**, *103*, 044314. [[CrossRef](#)]
41. Cai, B.; Chen, G.; Xu, J.; Yuan, C.; Qi, C.; Yao, Y. α decay half-life estimation and uncertainty analysis. *Phys. Rev. C* **2020**, *101*, 054304. [[CrossRef](#)]
42. Zhang, Z.Y.; Yang, H.B.; Huang, M.H.; Gan, Z.G.; Yuan, C.X.; Qi, C.; Andreyev, A.N.; Liu, M.L.; Ma, L.; Zhang, M.M.; et al. New alpha-emitting isotope ^{214}U and abnormal enhancement of alpha-particle clustering in lightest uranium isotopes. *Phys. Rev. Lett.* **2021**, *126*, 152502. [[CrossRef](#)]
43. Fukunishi, N.; Otsuka, T.; Sebe, T. Vanishing of the shell gap in $N = 20$ neutron-rich nuclei. *Phys. Lett. B* **1992**, *296*, 279–284. [[CrossRef](#)]
44. Utsuno, Y.; Otsuka, T.; Mizusaki, T.; Honma, M. Varying shell gap and deformation in $N \sim 20$ unstable nuclei studied by the Monte Carlo shell model. *Phys. Rev. C* **1999**, *60*, 054315. [[CrossRef](#)]
45. Caurier, E.; Nowacki, F.; Poves, A. Merging of the islands of inversion at $N = 20$ and $N = 28$. *Phys. Rev. C* **2014**, *90*, 014302. [[CrossRef](#)]
46. Chen, J.; Auranen, K.; Avila, M.L.; Back, B.B.; Caprio, M.A.; Hoffman, C.R.; Gorelov, D.; Kay, B.P.; Kuvín, S.A.; Liu, Q.; et al. Experimental study of the low-lying negative-parity states in ^{11}Be using the $^{12}\text{B}(d,^3\text{He})^{11}\text{Be}$ reaction. *Phys. Rev. C* **2019**, *100*, 064314. [[CrossRef](#)]
47. Chen, J.; Wang, S.M.; Fortune, H.T.; Lou, J.L.; Ye, Y.L.; Li, Z.H.; Michel, N.; Li, J.G.; Yuan, C.X.; Ge, Y.C.; et al. Observation of the near-threshold intruder 0^- resonance in ^{12}Be . *Phys. Rev. C* **2021**, *103*, L031302. [[CrossRef](#)]
48. Yang, Z.H.; Kubota, Y.; Corsi, A.; Yoshida, K.; Sun, X.X.; Li, J.G.; Kimura, M.; Michel, N.; Ogata, K.; Yuan, C.X.; et al. Quasifree neutron knockout reaction reveals a small s-orbital component in the Borromean nucleus ^{17}B . *Phys. Rev. Lett.* **2021**, *126*, 082501. [[CrossRef](#)]
49. Yuan, C.X. Impact of off-diagonal cross-shell interaction on ^{14}C . *Chin. Phys. C* **2017**, *41*, 104102. [[CrossRef](#)]

50. Jiang, Y.; Lou, J.L.; Ye, Y.L.; Liu, Y.; Tan, Z.W.; Liu, W.; Yang, B.; Tao, L.C.; Ma, K.; Li, Z.H.; et al. Quadrupole deformation of ^{16}C studied by proton and deuteron inelastic scattering. *Phys. Rev. C* **2020**, *101*, 024601. [CrossRef]
51. Yuan, C.X.; Suzuki, T.; Otsuka, T.; Xu, F.; Tsunoda, N. Shell-model study of boron, carbon, nitrogen, and oxygen isotopes with a monopole-based universal interaction. *Phys. Rev. C* **2012**, *85*, 064324. [CrossRef]
52. Wang, Y.B.; Su, J.; Han, Z.Y.; Tang, B.; Cui, B.Q.; Ge, T.; Lyu, Y.L.; Brown, B.A.; Yuan, C.X.; Chen, L.H. Direct observation of the exotic $\beta-\gamma-\alpha$ decay mode in the $T_z = -1$ nucleus ^{20}Na . *Phys. Rev. C* **2021**, *103*, L011301. [CrossRef]
53. Utsuno, Y.; Otsuka, T.; Brown, B.A.; Honma, M.; Mizusaki, T.; Shimizu, N. Shape transitions in exotic Si and S isotopes and tensor-force-driven Jahn-Teller effect. *Phys. Rev. C* **2012**, *86*, 051301. [CrossRef]
54. Nowacki, F.; Poves, A. New effective interaction for $0h\omega$ shell-model calculations in the $sd-pf$ valence space. *Phys. Rev. C* **2009**, *79*, 014310. [CrossRef]
55. Bazin, D.; Aoi, N.; Baba, H.; Chen, J.; Crawford, H.; Doornenbal, P.; Fallon, P.; Li, K.; Lee, J.; Matsushita, M.; et al. Spectroscopy of ^{33}Mg with knockout reactions. *Phys. Rev. C* **2021**, *103*, 064318. [CrossRef]
56. Gade, A.; Brown, B.A.; Tostevin, J.A.; Bazin, D.; Bender, P.C.; Campbell, C.M.; Crawford, H.L.; Elman, B.; Kemper, K.W.; Longfellow, B.; et al. Is the structure of ^{42}Si understood? *Phys. Rev. Lett.* **2019**, *122*, 222501. [CrossRef]
57. Hjorth-Jensen, M.; Kuo, T.T.S.; Osnes, E. Realistic effective interactions for nuclear systems. *Phys. Rep.* **1995**, *261*, 125–270. [CrossRef]
58. Brown, B.A. The nuclear shell model towards the drip lines. *Prog. Part. Nucl. Phys.* **2001**, *47*, 517–599. [CrossRef]
59. Noritaka, S. Nuclear shell-model code for massive parallel computation, “KSHELL”. *arXiv* **2013**, arXiv:1310.5431.
60. Noritaka, S.; Takahiro, M.; Yutaka, U.; Yusuke, T. Thick-restart block Lanczos method for large-scale shell-model calculations. *Comput. Phys. Commun.* **2019**, *244*, 372–384.
61. Available online: <https://sites.google.com/a/cns.s.u-tokyo.ac.jp/kshell/> (accessed on 1 November 2021).
62. Brown, B.A.; Richter, W.A.; Julies, R.E.; Wildenthal, B.H. Semi-empirical effective interactions for the $1s-0d$ shell. *Ann. Phys.* **1988**, *182*, 191–236. [CrossRef]
63. Kuo, T.T.S.; Brown, G.E. Reaction matrix elements for the $0f-1p$ shell nuclei. *Nucl. Phys. A* **1968**, *114*, 241–279. [CrossRef]
64. Millener, D.J.; Kurath, D. The particle-hole interaction and the beta decay of ^{14}B . *Nucl. Phys. A* **1975**, *255*, 315–338. [CrossRef]
65. Warburton, E.K.; Alburger, D.E.; Becker, J.A.; Brown, B.A.; Raman, S. Probe of the shell crossing at $A=40$ via beta decay: Experiment and theory. *Phys. Rev. C* **1986**, *34*, 1031–1051. [CrossRef]
66. Bansal, R.K.; French, J.B. Even-parity-hole states in $f7/2$ -shell nuclei. *Phys. Lett.* **1964**, *11*, 145–148. [CrossRef]
67. Doornenbal, P.; Scheit, H.; Takeuchi, S.; Utsuno, Y.; Aoi, N.; Li, K.; Matsushita, M.; Steppenbeck, D.; Wang, H.; Baba, H.; et al. Low- Z shore of the “island of inversion” and the reduced neutron magicity toward ^{28}O . *Phys. Rev. C* **2017**, *95*, 041301. [CrossRef]
68. Utsuno, Y.; Otsuka, T.; Glasmacher, T.; Mizusaki, T.; Honma, M. Onset of intruder ground state in exotic Na isotopes and evolution of the $N = 20$ shell gap. *Phys. Rev. C* **2004**, *70*, 044307. [CrossRef]
69. Han, R.; Li, X.Q.; Jiang, W.G.; Li, Z.H.; Hua, H.; Zhang, S.Q.; Yuan, C.X.; Jiang, D.X.; Ye, Y.L.; Li, J.; et al. Northern boundary of the “island of inversion” and triaxiality in ^{34}Si . *Phys. Lett. B* **2017**, *772*, 529–533. [CrossRef]
70. Honma, M.; Otsuka, T.; Mizusaki, T.; Hjorth-Jensen, M. Shell-model description of beta-decays for pf -shell nuclei. *Riken Accel. Prog. Rep.* **2009**, *42*, 43.
71. Otsuka, T.; Suzuki, T.; Honma, M.; Utsuno, Y.; Tsunoda, N.; Tsukiyama, K.; Hjorth-Jensen, M. Novel features of nuclear forces and shell evolution in exotic nuclei. *Phys. Rev. Lett.* **2010**, *104*, 012501. [CrossRef]
72. Poves, A.; Zuker, A. Theoretical spectroscopy and the fp shell. *Phys. Rep.* **1981**, *70*, 235–314. [CrossRef]
73. Bertsch, G.; Borysowicz, J.; McManus, H.; Love, W.G. Interactions for inelastic scattering derived from realistic potentials. *Nucl. Phys. A* **1977**, *284*, 399–419. [CrossRef]
74. Nummela, S.; Baumann, P.; Caurier, E.; Dessagne, P.; Jokinen, A.; Knipper, A.; Le Scornet, G.; Miehé, C.; Nowacki, F.; Oinonen, M.; et al. Spectroscopy of $^{34,35}\text{Si}$ by β decay: $Sd-fp$ shell gap and single-particle states. *Phys. Rev. C* **2001**, *63*, 044316. [CrossRef]
75. Retamosa, J.; Caurier, E.; Nowacki, F.; Poves, A. Shell model study of the neutron-rich nuclei around $N = 28$. *Phys. Rev. C* **1997**, *55*, 1266–1274. [CrossRef]
76. Kahana, S.; Lee, H.C.; Scott, C.K. Effect of Woods-Saxon wave functions on the calculation of $A=18, 206, 210$ spectra with a realistic interaction. *Phys. Rev.* **1969**, *180*, 956–966. [CrossRef]
77. Gloeckner, D.H.; Lawson, R.D. Spurious center-of-mass motion. *Phys. Lett. B* **1974**, *53*, 313–318. [CrossRef]
78. Kondev, F.G.; Wang, M.; Huang, W.J.; Naimi, S.; Audi, G. The NUBASE2020 evaluation of nuclear physics properties. *Chin. Phys. C* **2021**, *45*, 030001. [CrossRef]
79. Available online: <https://www.nndc.bnl.gov/nudat2/> (accessed on 1 November 2021).
80. Umeya, A.; Muto, K. Single-particle energies in neutron-rich nuclei by shell model sum rule. *Phys. Rev. C* **2006**, *74*, 034330. [CrossRef]
81. Yuan, C.X.; Qi, C.; Xu, F.R. Shell evolution in neutron-rich carbon isotopes: Unexpected enhanced role of neutron–neutron correlation. *Nucl. Phys. A* **2012**, *883*, 25–34. [CrossRef]
82. Otsuka, T.; Tsunoda, Y.; Abe, T.; Shimizu, N.; Van Duppen, P. Underlying Structure of Collective Bands and Self-Organization in Quantum Systems. *Phys. Rev. Lett.* **2019**, *123*, 222502. [CrossRef]
83. Yuan, C.X.; Liu, M.L.; Ge, Y.L. Shell-model explanation on some newly discovered isomers. *Nucl. Phys. R* **2020**, *37*, 447–454.